Computational and Structural Biotechnology Journal 21 (2023) 5451–5462

Contents lists available at ScienceDirect

Computational and Structural Biotechnology Journal

journal homepage: www.elsevier.com/locate/csbj

Research article

Candida antarctica lipase B performance in organic solvent at varying water activities studied by molecular dynamics simulations

Helena D. Tjørnelund [a], Jesper Vind [b], Jesper Brask [b], John M. Woodley [c], Günther H.J. Peters [a,*]

[a] Department of Chemistry, Technical University of Denmark, 2800 Kgs Lyngby, Denmark
[b] Novozymes A/S, 2800 Kgs Lyngby, Denmark
[c] Department of Chemical and Biochemical Engineering, Technical University of Denmark, 2800 Kgs Lyngby, Denmark

ARTICLE INFO

Keywords:
Biocatalysis
Candida *antarctica* lipase B (CALB)
Esterification
Protein engineering
Organic solvent
Water activity

ABSTRACT

Applications of lipases in low-water environments are found across a broad range of industries, including the pharmaceutical and oleochemical sectors. This includes condensation reactions in organic solvents where the enzyme activity has been found to depend strongly on both the solvent and the water activity (a_w). Despite several experimental and computational studies, knowledge is largely empirical, and a general predictive approach is much needed. To close this gap, we chose native *Candida antarctica* lipase B (CALB) and two mutants thereof and used molecular dynamics (MD) simulations to gain a molecular understanding of the effect of a_w on the specific activity of CALB in hexane. Based on the simulations, we propose four criteria to understand the performance of CALB in organic media, which is supported by enzyme kinetics experiments. First, the lipase must be stable in the organic solvent, which was the case for native CALB and the two mutants studied here. Secondly, water clusters that form and grow close to the active site must not block the path of substrate molecules into the active site. Thirdly, the lipase's lid must not cover the active site. Finally, mutations and changes in a_w must not disrupt the geometry of the active site. We show that mutating specific residues close to the active site can hinder water cluster formation and growth, making the lipase resistant to changes in a_w. Our computational screening criteria could potentially be used to screen *in-silico* designed variants, so only promising candidates could be pushed forward to characterisation.

1. Introduction

The ability of lipases (EC 3.1.1.3) to catalyse reactions in organic solvents was first discovered in the 1930s, [1–4] but it was not until the 1980s with Zaks and Klibanov's work on porcine pancreatic lipase in 2-pentanone that the field took off. [5,6] Since then, lipases have been incorporated into a broad range of different industries, including the oleochemical, biofuel, pharmaceutical, food, and agrochemical sectors. [7–12] Lipases are favoured as biocatalysts because of their high substrate specificity and regio-, chemo-, and enantioselectivity not only in hydrolysis, but also in *e.g.* esterification, transesterification, alcoholysis, and aminolysis reactions [13–15].

Numerous reports have shown that the enzymatic activity of lipases is highly correlated with the type of reaction medium and the reaction medium's water content, which is often reported as water activity (a_w). [16–19] In synthesis reactions (condensations, transacylations), water content is kept low to minimise hydrolysis. However, exhaustive drying can also inactivate certain lipases, presumably as essential water molecules needed for protein flexibility are stripped from the protein. [20] The effects of a_w on lipase activity depend strongly on the lipase. The esterification rate of most lipases increases with increasing a_w, as seen for *Candida rugosa* and *Pseudomonas cepacia*, while other lipases display a bell-shaped activity profile. [17,19] This indicates that even at high a_w, the esterification reaction is still dominant. Quite exceptionally, *Candida antarctica* lipase B (CALB) and *Bacillus subtilis* lipase exhibit a decrease in enzymatic activity when a_w increases [21–23].

To date, several studies have investigated various enzymes in different organic media using a combination of experimental methods

Abbreviations: ACN, acetonitrile; CALB, *Candida antarctica* lipase B; GAFF2, General AMBER force field 2; MD, molecular dynamics; MTBE, methyl *tert*-butyl ether; PDB, Protein Data Bank; R_g, radius of gyration; RMSD, root-mean-squared deviation; RMSF, root-mean-squared fluctuation; SASA, solvent accessible surface area; TI, thermodynamic integration; a_w, water activity.

* Corresponding author.
E-mail address: ghp@kemi.dtu.dk (G.H.J. Peters).

https://doi.org/10.1016/j.csbj.2023.10.049
Received 8 September 2023; Received in revised form 27 October 2023; Accepted 27 October 2023
Available online 31 October 2023

and computational techniques such as molecular dynamics (MD) simulations; this interdisciplinary approach provides an avenue to understand how lipases are affected by the solvent composition on an atomic level. A recent study on lipase A from *Bacillus subtilis* in water, acetonitrile (ACN), dimethyl sulfoxide, and isopropyl alcohol using fluorescence resonance energy transfer and MD simulations revealed two main factors governing the enzymatic activity. [24] First, the organic solvent displayed competitive binding to the active site, displacing the substrate molecules, and secondly, the organic solvents changed the geometry of the active site. The competition between substrate and solvent molecules has previously been shown to affect lipase activity. [25] The authors studied CALB in ACN, methyl *tert*-butyl ether (MTBE), *tert*-butyl alcohol, and hexane and found a linear correlation between $\ln(V_{max}/K_m)$ and the interaction energies between the solvent molecules and residues in the active site pocket. [25] Other studies have proposed that enzyme activity is correlated to the enzyme's flexibility, which is connected to the solvent's log(P). [26,27] A computational study by Trodler and Pleiss showed that the flexibility of CALB decreased with increasing log (P)-values of the solvents (water, methanol, chloroform, toluene, and cyclohexane) [28].

CALB is, to this day, one of the most used lipases in the industry because of its broad range of substrates, high enantioselectivity, thermostability, and stability in organic solvents. [29] We have previously shown that the activity of CALB in organic solvents is highly correlated with the reaction medium's a_w, as CALB's specific activity decreases with increasing a_w. [22] This correlation is seen in multiple solvents, including ACN, MTBE, and hexane, which have different physical and chemical characteristics, such as functional groups and log(P). Another study investigated CALB in MTBE at four different water activities using enzyme kinetics and MD simulations. The authors showed that water clusters are present at specific regions (referred to as 'hot-spot' regions) on the protein surface and that they grow with increasing a_w. [23] The authors identified a 'hot-spot' region located close to the entrance of CALB's active site groove and hypothesised that this water cluster can sterically hinder the path of substrate molecules to the active site and hence, may explain why CALB loses enzymatic activity at high a_w. [23] It has been shown that in every 'hot-spot' region, one or more residues can form hydrogen bonds to the water molecules. [23] In the 'hot-spot' region close to the active site, the two acidic residues, Glu^{188} and Asp^{223}, form hydrogen bonds to the water molecules, and we believe that these act as a nucleation site for the water cluster formation.

To investigate the influence of Glu^{188} and Asp^{223} on water cluster formation, we designed two CALB mutants *in-silico* and studied them using MD simulations. In the first mutant, E188Q+D223N, the acidic residues were mutated to glutamine and asparagine. In the second mutant, E188Q+D223L, besides removing the acidic residues, the ability of aspartic acid's side chain to form hydrogen bonds with surrounding water molecules was removed by mutating it to leucine. These mutations were chosen since the residues have a similar structural skeleton and would be less invasive compared to other residues, thereby not affecting the enzyme structure negatively. Native CALB (hereafter referred to as $CALB^{native}$) and two CALB mutants (E188Q+D223N and E188Q+D223L; hereafter referred to as $CALB^{E188Q+D223N}$ and $CALB^{E188Q+D223L}$, respectively) were investigated at three water activities in hexane using MD simulations. The computational study revealed that in addition to water cluster formation, the lid conformation and the active site's geometry also influence the lipase activity. To support the computational findings, the activities of $CALB^{native}$ and the mutants were determined using an in-house assay, where the esterification reaction between butyric acid and ethanol was used as a model system [22].

2. Materials and methods

2.1. In-silico studies

The physicochemical properties of $CALB^{native}$ and the two CALB mutants, $CALB^{E188Q+D223N}$ and $CALB^{E188Q+D223L}$, were investigated at an atomic level using MD simulations. The lipases were simulated for 100 ns in hexane with a varying number of water molecules, and the simulations were made as triplicates. The lipases were simulated with 100, 200, and 300 water molecules to represent low, medium, and high a_w. After the MD simulations, the water activities in the simulation systems could be calculated using the protocol designed by Wedberg and co-workers. [30] Additional simulations were performed for a pure hexane system as well as for $CALB^{native}$ and the CALB mutants in complex with a substrate (butyric acid). All simulations were carried out in AMBER18 [31].

2.1.1. System preparation

The three-dimensional structure of a hexane molecule was retrieved from PubChem, and the atom types were assigned by the General AMBER Force Field 2 (GAFF2). [32,33] The atomic point charges were calculated using the AM1-BCC charge model with Antechamber, which is a part of AMBERTOOLS. [31] 3119 hexane molecules were placed in a cubic box with a side length of 90 Å using PackMol. [34] The energy of the solvent box was minimised using single-point energy calculations, where initially, 1000 steps with the steepest descent method were performed, followed by 4000 steps of conjugated gradient minimisation. Afterwards, the solvent box was heated to 298.15 K during a 1 ns long MD simulation in the *NVT* (N = constant number of atoms, V=constant volume, T = constant temperature) ensemble. Lastly, the system was equilibrated for 1 ns during an *NpT* (N = constant number of atoms, p = constant pressure, T = constant temperature) MD simulation. The MD simulation details for the heating and equilibration are given in Section 2.1.2. The solvent box's density after minimisation, heating, and equilibration was 0.665 ± 0.002 g/mL, which is in good agreement with the experimental density of hexane at 25 °C (0.66 g/mL) [32].

CALB consists of 317 residues and belongs to the α/β hydrolase-fold family with 10 α-helices and 7 β-strands. [35,36] Its active site consists of the catalytic triad Ser^{105}, Asp^{187}, and His^{224}. The crystal structure of CALB retrieved from the Protein Data Bank (PDB: entry 5A71) with a resolution of 0.91 Å was used in the MD simulations. [35,37] The crystal structure was cleaned in PyMOL (version 2.4.1, Schrödinger, LLC) so that only chain A, which corresponds to the open conformation of CALB, and the 533 water molecules belonging to chain A were kept. The water molecules with the highest B-factors were deleted to obtain the desired number of water molecules. In addition, a proline was added to the C-terminus using the Builder module in PyMOL before the model for the native structure was saved. To prepare the mutants, the native model was loaded into PyMOL, and the Mutagenesis module was used to implement the point mutations at positions 188 and 223 before the models were saved. The models were protonated in H++ (version 3.0, http://biophysics.cs.vt.edu/H++). [38–40] The calculations were carried out at pH 7.0 with a salinity of 0.0 M, an internal dielectric constant of 10, and an external dielectric constant of 1.89, corresponding to hexane. [41] H++ computed Glu^{188} and Asp^{223} to be deprotonated and protonated, respectively, in the native model. The resulting coordination and topology files were saved and converted into PDB-format using ambpdb, which is part of AMBERTOOLS. In accordance with Stauch and co-workers, Asp^{134} and Asp^{145} were protonated, while the active site histidine (His^{224}) was single protonated with a proton at the δ-nitrogen. [35] The water molecules were lost during the calculations in H++; however, these were re-added to the models using PyMOL. To build the

simulation systems, the protonated proteins with water molecules were loaded into PyMOL together with the prepared solvent box of hexane. The proteins were placed in the solvent box's centre, and hexane molecules within 3 Å of the protein were deleted so that the final systems consisted of 2735 hexane molecules. Before the models were saved, two chloride ions were placed in the solvent box with $CALB^{native}$, and three chloride ions were placed in the solvent boxes with $CALB^{E188Q+D223N}$ and $CALB^{E188Q+D223L}$ to neutralise the systems. Afterwards, the residue and atom numbers were corrected using pdb4amber. The protein force field ff14SB, GAFF2, and the TIP3P water model were assigned to the models using LEaP. [42,43] The AMBER force fields were chosen in this study, as they have previously been used to study lipases in organic solvents [28,44].

2.1.2. Molecular dynamics simulations of lipase in organic solvent

The simulation systems consisting of lipase, water, chloride ions, and hexane molecules were first energy minimised to remove possible bad contacts between atoms. [45] The number of minimisation steps was varied to achieve different starting conformations in the triplicate simulations. Simulation 1, simulation 2, and simulation 3 consisted of 1000, 1500, and 1800 steepest descent cycles followed by 4000, 3500, and 3200 conjugated gradient cycles, respectively. During minimisation, a positional restraint of 10.0 kcal/(mol·Å^2) was placed on the protein backbone atoms [31].

After the energy minimisation, the systems were heated to 298.15 K using the *NVT* ensemble. The temperature was increased linearly to 298.15 K for 0.3 ns and afterwards kept at 298.15 K for 0.7 ns. The temperature was controlled with the Langevin thermostat, where a collision frequency of 5.0 ps^{-1} was employed, and the initial velocities were generated using a pseudo-random number [46].

Following the heating step, the systems were equilibrated for 4 ns using the *NpT* ensemble. The temperature was kept constant using the Langevin thermostat, where a collision frequency of 1.0 ps^{-1} was employed, while the Monte Carlo barostat was used to control the pressure. [47] Lastly, 100 ns long production runs were performed under the same conditions as in the equilibration. The trajectories from the production runs were subsequently used in the analyses. During the minimisation and MD simulations, a cut-off of 12 Å was employed for the non-bonded interactions, while the particle mesh Ewald method [48] was employed for the electrostatic interactions. Additionally, the SHAKE algorithm was used to constrain the lengths of bonds with hydrogen atoms allowing a time step of 0.002 ps. [49] The simulations were performed with periodic boundary conditions in all three Cartesian coordinates.

2.1.3. Docking and MD simulations of lipase-substrate complexes

A two-dimension model of a protonated butyric acid molecule was drawn using 2D Sketcher in Maestro (Schrödinger Release 2022–4, Schrödinger, LLC, USA), and the atom types and bond lengths were assigned by the OPLS4 force field. [50] Representative structures of each lipase at the three water activities (subsection 2.1.4) were used for the docking studies, which were carried out in Glide. [51,52] The receptor grids were prepared using an enclosed box with centre in Ser^{105}, where the hydroxyl group of Ser^{105} was allowed to rotate. Afterwards, the protonated butyric acid molecule was docked into the receptors using Extra Precision (XP) mode and flexible ligand sampling. The dockings were performed without any constraints, with 0.15 partial charges cut off, and 0.80 van der Waals radius scaling. The docking runs were followed by a short minimisation performed using the default Glide settings. The lipase-substrate complexes were saved as PDB-files, and placed in the hexane solvent box, where hexane molecules within 3 Å of the protein were deleted using PyMOL. Similar to the previous setups, the systems were neutralised with two chloride ions for $CALB^{native}$, and three chloride ions for $CALB^{E188Q+D223N}$ and $CALB^{E188Q+D223L}$. The atom types for butyric acid were prior to the MD simulations assigned by GAFF2, and the point charges were calculated using the AM1-BCC charge model. Likewise, ff14SB, GAFF2, and the TIP3P water model were assigned to the systems using LEaP. The systems were simulated in triplicates using the same procedure as for the previous MD simulations, with only two changes: (*i*) a positional restraint of 100 kcal/(mol·Å^2) was placed on butyric acid and the active site residues (Ser^{105}, Asp^{187}, and His^{224}) during the minimisation, heating, and equilibration steps to allow for proper alignment between butyric acid and residues in the active site region of the enzyme (note: restraint was not applied during production run) and (*ii*) the length of the production run was 20 ns (note: the last 15 ns of the production run was used in the subsequent analyses).

2.1.4. Analyses

The trajectories from the MD simulations of the $CALB^{native}$ and the two CALB mutants were analysed using a combination of CPPTRAJ [53], which is part of AMBERTOOLS, and VMD (version 1.9.1) [54]. The stability of the simulations was investigated by calculating the backbone atoms' root-mean-squared deviation (RMSD) with respect to the minimised structures using CPPTRAJ. Protein flexibility was deduced from the average root-mean-squared fluctuations (RMSFs) of the backbone atoms using CPPTRAJ. Representative structures of the models were extracted from the simulations using hierarchical agglomerative clustering in CPPTRAJ. The triplicate simulations of a lipase at a given a_w were pooled, and the conformations were clustered based on the backbone atoms' RMSDs. The clustering was stopped when only ten clusters remained. The conformation closest to the biggest centroid of the cluster was denoted as the representative structure and used for further analysis. The number of water molecules in contact with the protein was calculated using in-house VMD script.

2.1.5. Water activity calculation

After it had been established that the simulations had converged, a_w of each simulation system was calculated using the last 10 ns of the simulations. [30] The a_w cannot be determined prior to a simulation, as it is calculated from the ratio of water molecules close to the protein surface and water molecules in the bulk solvent. [30] The border between the bulk and protein proximity region is determined with Eq. 1.

$$x_w(r) = \frac{\langle N_w(r)\rangle}{\langle N_w(r)\rangle + \langle N_s(r)\rangle} \quad (1)$$

Here, $N_w(r)$ and $N_s(r)$ represent the time-averaged ($\langle\ldots\rangle$) number of water and solvent molecules in a region from r-0.25 Å to r + 0.25 Å, where r is the distance to the protein surface. The distance was measured from the oxygen atom in water and the third carbon atom in hexane. $x_w(r)$ is the water mole fraction, which will converge to a constant value (bulk water) when plotted against r. The smallest r, where $x_w(r)$ is still constant will define the border to the bulk region; Fig. S1 presents the water mole fraction plots for $CALB^{native}$. Then a_w is given by $a_w = \gamma_w(x_w)\cdot x_w$, where $\gamma_w(x_w)$ is the activity coefficient for a binary solution at a given x_w. As described by Wedberg and co-workers, $\gamma_w(x_w)$ can be approximated by the activity coefficient at infinite dilution (γ_w^{∞}), when x_w is below 0.02. [30] In this study, all the simulations were performed at x_w below 0.02. The activity can be described by the chemical potentials of the mixture (μ_w) and the pure state (μ_w^o).

$$k_B\cdot T\cdot\ln(x_w\gamma_w) = \mu_w - \mu_w^o \quad (2)$$

Employing Widom's method on the chemical potentials, Eq. 2 can be rewritten to the following [55].

$$k_B \cdot T \cdot \ln(x_w \gamma_w) = \Delta G_{solv} - \Delta G_{water} + k_B \cdot T \cdot \ln\left(\frac{\rho_w}{\rho_w^o}\right) \quad (3)$$

In the limit, where $x_w \rightarrow 0$, i.e. at infinite dilution, Eq. 3 becomes:

$$\ln\gamma_w^{\infty} = \frac{\Delta G_{solv} - \Delta G_{water}}{k_B \cdot T} + \ln\left(\frac{\rho_{solv}^o}{\rho_{water}^o}\right) \quad (4)$$

Here, ΔG_{solv} and ΔG_{water} represent the Gibbs free energy of introducing one water molecule into an organic solvent and water, respectively, ρ_{solv}^o and ρ_{water}^o (mol/dm^3) are the molar densities of pure organic solvent and water, respectively, and T and k_B are the absolute temperature and Boltzmann constant, respectively.

ΔG_{solv} and ΔG_{water} can be calculated using thermodynamic integration (TI), where the interactions between the solute and solvent are gradually decoupled by varying the interaction parameter (λ). The decoupling of the solute molecule was performed as a two-step protocol. First, the electrostatic interactions from the outgoing water molecule were decoupled by gradually removing the atomic partial charges as λ increased from 0 to 1. Second, the Lennard-Jones interactions were gradually decoupled from the non-charged solute molecule using the linear mixing soft-core scaling implemented in AMBER with the α constant set to 0.5 as λ increased from 0 to 1. [56] The procedure was as follows; one water molecule was introduced into a solvent box with 500 hexane molecules or 999 water molecules. The simulation systems were prepared at λ = 0.5. First, the systems were minimised by 500 steepest descent minimisation steps. The temperature was then increased to 298.15 K during a 500 ps *NVT* simulation, where the Langevin thermostat with a collision frequency of 5.0 ps^{-1} and positional restraint of the atom (5.0 kcal/(mol·Å^2)) were employed. [46] Afterwards, the systems were equilibrated for 500 ps in the *NpT* ensemble using the Langevin thermostat (collision frequency of 2.0 ps^{-1}) and the Monte Carlo barostat [47].

Two series of simulations were performed for each system to ensure statistical significance. The two simulation series were started from different configurations obtained from the equilibration after 400 ps and 500 ps. TI for the solvation energies was based on twenty-four MD simulations where only λ varied (λ = 0, 0.05,…,0.95, 0.975, 0.99, 0.999, 1). The systems were equilibrated for 100 ps before a 1 ns production run was performed, where the temperature and pressure were controlled using the Langevin thermostat (collision frequency of 2.0 ps^{-1}) and Monte Carlo barostat. [46,47] TI yielded a solvation energy of $\Delta G_{solv,water} = -6.093 \pm 0.004$ kcal/mol and $\Delta G_{solv,hexane} = 0.8 \pm 0.1$ kcal/mol for water and hexane, respectively. In addition, the simulations yielded a density of 54 ± 2 mol/dm^3 for water and 7.66 ± 0.03 mol/dm^3 for hexane, which are close to the experimental densities of 55.21 mol/dm^3 and 7.6 ± 0.3 mol/dm^3. [57] Inserting the given densities and solvation energies in Eq. 4 yielded: $\ln(\gamma_w^{\infty}) = 9.69 \pm 0.05$. Table 1 summarises the number of water molecules used in each MD simulation and the resulting a_w. To test how the length of the MD simulations affects the calculated water activities, the simulations for CALB$^{E188Q+D223L}$ with 300 water molecules were extended from 100 ns to 400 ns. Noticeably, the length of the simulation did not affect a_w, which was determined to be 0.9 ± 0.4 at both 100 ns and 400 ns.

2.2. Experimental procedure

The initial water activities were set, and the lipases' specific activities were measured using our previously described method. [22] The specific activities were determined using the esterification reaction between butyric acid and ethanol yielding ethyl butyrate.

2.2.1. Chemicals

CALB^{native}, CALB$^{E188Q+D223N}$, and CALB$^{E188Q+D223L}$ were provided by Novozymes A/S (Bagsværd, Denmark). Butyric acid, ethanol absolute, ethyl butyrate, HCl, hexane (≥98%), 1-hexanol, lithium chloride (LiCl), magnesium nitrate hexahydrate ($Mg(NO_3)_2 \cdot 6\ H_2O$), and potassium sulfate (K_2SO_4) were purchased from Sigma-Aldrich GmbH (Steinheim, Germany). All chemicals were of analytical grade except hexane, which was of gas chromatographic grade.

2.2.2. Protein preparation

CALB$^{E188Q+D223N}$ and CALB$^{E188Q+D223L}$ were cloned, expressed, and purified as previously reported. [58] CALB^{native} was isolated from commercial Lipozyme CALB L. Prior to enzyme kinetics experiments, the lipases were transferred to phosphate buffer (10 mM NaH_2PO_4, 140 mM NaCl, 27 mM KCl, pH 7.0) by dilution of the original buffer (approx. 8000x) and concentrated using a 10 kDa spin filter (Vivaspin Turbo 4, Sartorius, UK). The theoretical extinction coefficients (41285 M^{-1} cm^{-1}) were calculated with the ExPASy server using the protein sequences. [59] The protein concentrations were measured in triplicates on an ND-1000 NanoDrop Spectrophotometer (Thermo Fischer Scientific, USA) at 280 nm. The concentrations were 35 mg/mL, 6.25 mg/mL, and 1.72 mg/mL for CALB^{native}, CALB$^{E188Q+D223N}$, and CALB$^{E188Q+D223L}$, respectively. The three lipases were aliquoted and stored at − 20 °C.

2.2.3. Enzyme kinetics assay

CALB^{native} (0.53 mg), CALB$^{E188Q+D223N}$ (0.5 mg), or CALB$^{E188Q+D223L}$ (0.25 mg) were mixed with organic reaction medium (5 mL) consisting of hexane with 50 mM butyric acid. The reaction medium with lipases was pre-equilibrated for 24 h above saturated salt solutions to set the initial a_w. [22] The three salts LiCl ($a_w = 0.12$), $Mg(NO_3)_2 \cdot 6\ H_2O$ ($a_w = 0.53$), and K_2SO_4 ($a_w = 0.97$) were used for the salt solutions. After the pre-equilibration, the volume of the reaction medium was corrected, and ethanol was added to initiate the enzymatic

Table 1
Results from MD simulations of the lipases at different water activities.

Lipase	Number of H_2O[a]	a_w	Alignment RMSD (Å)[b]	Simulation RMSD (Å)[c]	SASA (Å^2)* 10^3[c]	R_g (Å)[c]
CALB^{native}	100	0.09 ± 0.04	—	0.95 ± 0.06	10.8 ± 0.2	18.03 ± 0.02
	200	0.6 ± 0.4	0.81	0.9 ± 0.3	11.1 ± 0.1	18.06 ± 0.03
	300	1.00 ± 0.09	0.86	0.8 ± 0.1	11.16 ± 0.01	18.05 ± 0.03
CALB$^{E188Q+D223N}$	100	0.05 ± 0.03	0.81	1.1 ± 0.2	10.8 ± 0.2	18.08 ± 0.05
	200	0.6 ± 0.1	0.86	0.8 ± 0.1	11.1 ± 0.1	18.06 ± 0.03
	300	1.1 ± 0.3	0.88	0.86 ± 0.07	11.1 ± 0.1	18.04 ± 0.03
CALB$^{E188Q+D223L}$	100	0.15 ± 0.07	0.79	0.83 ± 0.06	10.8 ± 0.1	18.03 ± 0.03
	200	0.6 ± 0.4	0.74	1.0 ± 0.2	11.1 ± 0.1	18.07 ± 0.03
	300	0.9 ± 0.4	0.83	0.75 ± 0.03	11.1 ± 0.3	18.04 ± 0.01

[a] 100, 200, and 300 water molecules correspond to low, medium, and high water activities, respectively.
[b] Structural alignment of the lipases' representative structures to the representative structure of CALB^{native} at low water activity (100 H_2O). The alignment was made in PyMOL.
[c] RMSDs, SASAs, and R_gs are calculated from the MD simulations. RMSDs are calculated with respect to the minimised structures.

reactions. [22] The concentration of ethanol in the reaction medium was 50 mM. At given time intervals, 100 μL samples were taken from the reaction flask, and the enzymatic reaction was stopped using 1 M HCl (10 μL). The produced amount of ethyl butyrate in the samples were analysed using a Perkin Elmer Clarus 500 gas chromatograph (Shelton, Connecticut, USA) with a flame ionisation detector, and 1-hexanol was used as an internal standard. [22] The samples were injected into the gas chromatograph using split injection with a ratio of 1:50 and an injector temperature of 200 °C. The components were separated using a Nukol column (15 m length, 0.31 mm i.d., and 0.25 μm d_f) with the following temperature gradient. Initially, the column was kept at 50 °C for 5 min, then the temperature was raised to 100 °C using a temperature ramp of 25 °C/min and kept at 100 °C for 2 min. Afterwards, the temperature was increased at a rate of 25 °C/min to 175 °C and kept at 175 °C for 2 min. The detector was kept at 260 °C. Helium (0.75 mL/min) was used as the carrier gas. The specific activities (mmol/min/mg) were calculated from the initial reaction rate (mmol/mL/min) multiplied by the reaction volume (mL) and divided by the amount of enzyme (mg). Only the first 10% of the reaction (based on substrate conversion) was included in the calculations to ensure linearity [60].

3. Results and discussion

We have previously shown that the rate of lipase-catalysed esterification reactions with CALB decreases with increasing a_w, which is a quite unique feature for a lipase, and hypothesised that the lipase activity is affected by water cluster formation on the protein surface close to the active site, which may hinder the path of substrate molecules into the active site. [22,23] Two acidic residues (Glu^{188}, Asp^{223}) close to the active site region have been identified as the nucleation site for the

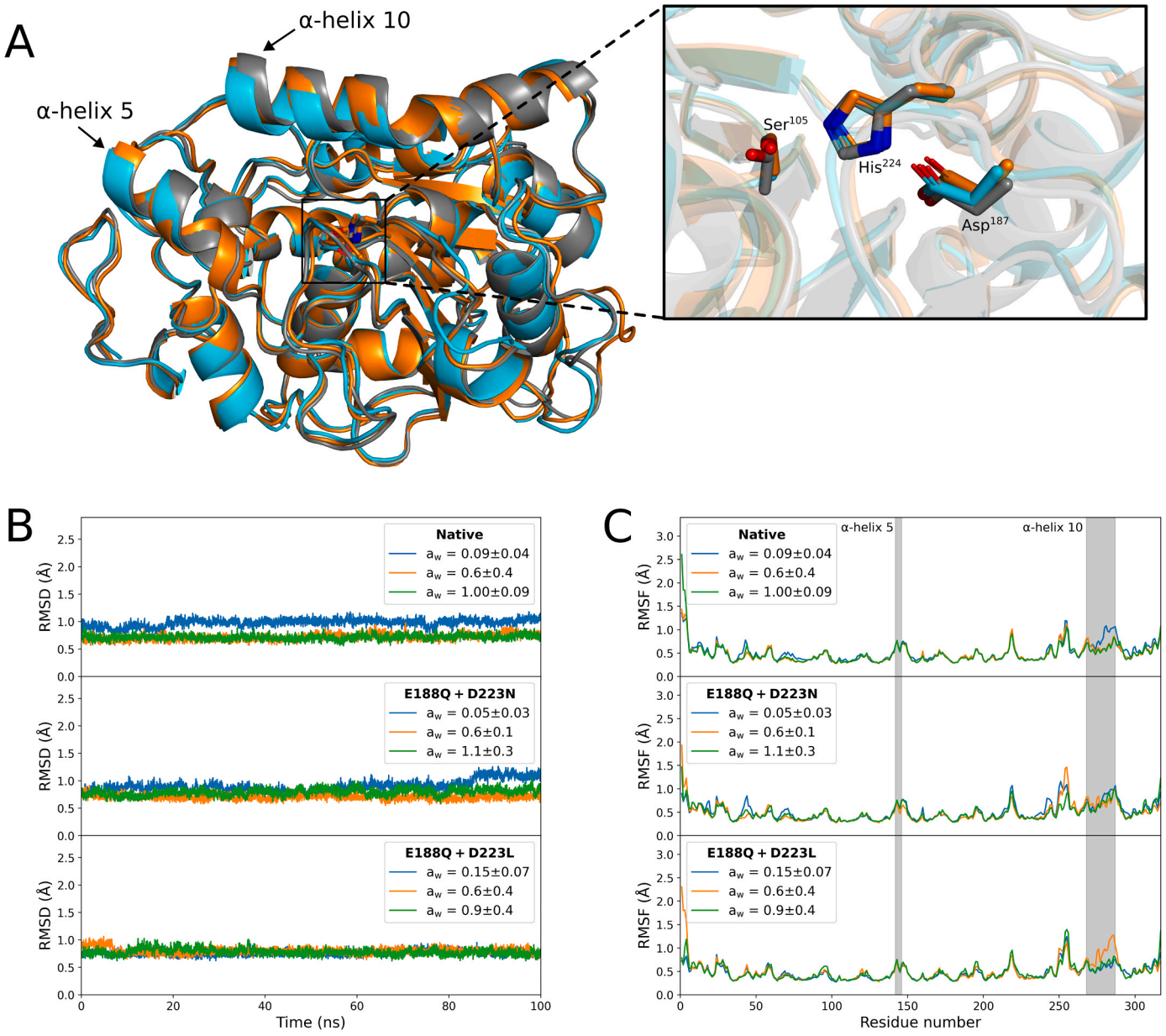

Fig. 1. Structural analysis of $CALB^{native}$, $CALB^{E188Q+D223N}$, and $CALB^{E188Q+D223L}$ at varying a_w (given in the inset). (A) Structural alignment of the representative structures of $CALB^{native}$ and the CALB mutants at low a_w (100 H_2O). The structures of $CALB^{native}$, $CALB^{E188Q+D223N}$, and $CALB^{E188Q+D223L}$ are represented as ribbons and colored in grey, blue, and orange, respectively. Zoom-in on the active site residues. All structures are in the open conformation, which is defined by the distance between α-helix 5 and α-helix 10. [35,58] (B) Time evolution of the RMSD of the backbone atoms. (C) Average RMSFs of the backbone atoms based on the triplicate simulations. The residues in α-helix 5 and α-helix 10 are marked by grey bars.

water cluster formation. To test the hypothesis, we designed two CALB mutants with double mutations ($CALB^{E188Q+D223N}$, $CALB^{E188Q+D223L}$) and studied their physicochemical properties using MD simulations. The MD simulations revealed that the lipases' activities were also governed by the lid conformation and the active site's geometry. The computational results were supported by experimentally determined specific activities calculated from the initial reaction rates of $CALB^{native}$ and the two mutants using an in-house assay [22].

3.1. Molecular dynamics simulations

Each variant was simulated in triplicates for 100 ns at three different water activities in hexane. Based on previous mechanistic studies of enzymes, we investigated four criteria that could affect lipase-catalysed reactions in low water environments: (*i*) Lipases must be stable in the organic solvent; [13,61,62] (*ii*) water clusters on the protein surface must not sterically hinder the entrance of substrate molecules into the active site; [23] (*iii*) lipases must remain in an open conformation, so the substrate molecules can enter the active site; [58,63,64] and (*iv*) the active site must remain in a catalytically competent conformation. [65–67] The four criteria are discussed in the following sections.

3.1.1. Criterion 1: Stability

The first part of the computational analysis was to investigate if $CALB^{native}$ and the two mutants underwent conformational changes during the MD simulations in hexane. RMSDs and RMSFs were used to study global movements and local flexibility in $CALB^{native}$ and the CALB mutants, respectively. Fig. 1 and Table 1 summarise the results, and as seen, $CALB^{native}$ and the two mutants have highly similar RMSD and RMSF values. The RMSDs of $CALB^{native}$ and the mutants are around 1 Å and stable throughout the simulations, indicating that the mutations and organic solvent do not introduce significant conformational changes. Low RMSDs have also been reported by Trodler and Pleiss for CALB in isopentane and cyclohexane (between 0.7 and 0.9 Å). [28] In addition, crystal structures of proteins soaked in organic solvents have shown that the structures do not differ from the structures obtained in water. [68,69] The low RMSDs are reflected in the low RMSF values, where most residues have an RMSF below 1 Å. The most flexible part of $CALB^{native}$ and the mutants is the N-terminus. The results for $CALB^{native}$ are in agreement with previous studies that have shown that $CALB^{native}$'s global structure is stable in hexane. [44,70] Noticeably, the global structures of $CALB^{native}$ and the two CALB mutants behave almost identically during the simulations at the three water activities. The radii of gyration (R_g) and solvent accessible surface areas (SASAs) were calculated to investigate changes in the global surface characteristics of the lipases. The SASA and R_g values for $CALB^{native}$ and the two CALB mutants are very similar at the different water activities (Fig. S2), which indicate that the mutations and a_w do not affect the global surface characteristics of CALB. The latter has also been observed for CALB in *tert*-butanol, MTBE, ACN, and hexane. [25] We also see that the structures resulting from the MD simulations are very similar when aligned (Fig. 1A and Table 1) indicating that $CALB^{native}$ and the two mutants should be stable in hexane. To test if 100 ns long MD simulations were proficient to show that the structural integrity is maintained, 400 ns long MD simulations were made for $CALB^{E188Q+D223L}$ at $a_w = 0.9 \pm 0.4$. As seen in Fig. S3, the mutant's RMSD, RMSF, SASA, and R_g remained stable and similar to those deduced from the 100 ns long simulations, indicating that the mutant is stable in hexane even in the extended simulations.

3.1.2. Criterion 2: Limited water cluster formation

The next step of the computational analysis was to investigate the environment around the active site before and after the point mutations of Glu^{188} and Asp^{223}. These two residues are of interest, since they are located close to the active site region, and as reported previously, the residues may act as the nucleation sites ('hot-spots') for the growth of a water cluster (Fig. 2A, B) that potentially sterically hinder the entry of substrate molecules. [23] When a_w is increased, the number of water molecules around the two residues also increases. We, therefore, hypothesised that mutating these two residues could limit the water cluster formation and, thereby, the lipase activity's dependency on a_w. As presented in Fig. 2C and Fig. 2D, mutating Glu^{188} and Asp^{223} to the corresponding amides still made it possible for the residues to form hydrogen bonds with the water molecules. However, the formed water clusters at low and high a_w were significantly smaller than the water clusters observed for $CALB^{native}$. When Asp^{223} is mutated to leucine, the ability for its side chain to form hydrogen bonds is removed (Fig. 2E and Fig. 2F).

The analysis in Fig. 2 is based on the last frame of the MD simulations to visualise the change in the water cluster formation caused by the point mutations. To quantify this change, the water molecules were tracked during the 100 ns long simulations. The results from the analysis are presented in Fig. 3 and Fig. S4. The number of water molecules around the active site and Glu^{188} and Asp^{223} increases with increasing a_w for the $CALB^{native}$. At low a_w, Glu^{188} and Asp^{223} are, on average, in contact with 3.6 ± 0.4 and 4.5 ± 0.6 water molecules, respectively, and the numbers increase to 3.9 ± 0.2 and 6.7 ± 0.9 at higher a_w values. In contrast, the number of water molecules around the two mutated residues is lower for the CALB mutants. $CALB^{E188Q+D223N}$ has, respectively, 1.0 ± 0.6 and 3.4 ± 0.5 water molecules around residue 188 and residue 223 at low a_w, which remains within the same uncertainty at higher a_w (residue 188: 0.5 ± 0.3 and residue 223: 3.3 ± 0.4). Similarly, the increase in water molecules for $CALB^{E188Q+D223L}$ is limited; for residue 188 and residue 223, the number increases from 1.4 ± 0.3 to 1.8 ± 0.2 and from 3.4 ± 0.3 to 3.88 ± 0.09 water molecules, respectively. Based on the reduced water cluster formation observed in $CALB^{E188Q+D223N}$ and $CALB^{E188Q+D223L}$ we hypothesise that the mutants should not be negatively affected by high a_w compared to $CALB^{native}$.

3.1.3. Criterion 3: Lid movement and open conformation

Skjøt and co-workers presented a 10 ns long MD simulation of CALB in explicit water, where they observed that α-helix 5 (residues 142–146) displayed high flexibility and that the helix moved closer to α-helix 10 (residues 268–287). [58] The displacement of α-helix 5 towards α-helix 10 correlates well with Stauch and co-workers' crystallographic work, which revealed that α-helix 5 and α-helix 10 are responsible for the closed conformation of CALB. [35] When CALB moves into the closed conformation, several interactions and conformational changes occur, amongst others α-helix 5 becomes an unstructured loop, where Asp^{145} loses its interactions with Ser^{150} (observed in the open conformation) and comes closer to Lys^{290} (closed conformation). [35,58] Inspired by the two studies, the lid conformations during the MD simulations were investigated. Fig. 1A and Fig. 1C show that, in contrast to the results of Skjøt and co-workers, no movement and structural change of the backbone atoms in α-helix 5 are observed in any of our 100 ns simulations. The side chain distance between Asp^{145} and Ser^{150} remains around 3.75 Å in $CALB^{native}$ and $CALB^{E188Q+D223L}$, which corresponds to the lid being in the open conformation (Fig. 4). The distance increases to around 7.0 Å in $CALB^{E188Q+D223N}$ at low and high a_w (Fig. 4), which resembles a more closed conformation according to Skjøt and co-workers. [58] The distance between Asp^{145} and Ser^{150} in $CALB^{E188Q+D223N}$ fluctuates throughout the simulations between an open and closed conformation and hence, the lid movement only partially provides access of the substrate to the active site region (Fig. S5).

The lid movement in $CALB^{E188Q+D223N}$ indicates that this variant may have a lower enzyme activity compared to $CALB^{E188Q+D223L}$ at low and high a_w.

3.1.4. Criterion 4: Optimal geometry of the active site

The final analysis of $CALB^{native}$ and the two CALB mutants focused on the geometry of the active site and was inspired by the recent work on lipase A from *Bacillus subtilis*. [24] Only when a catalytically competent

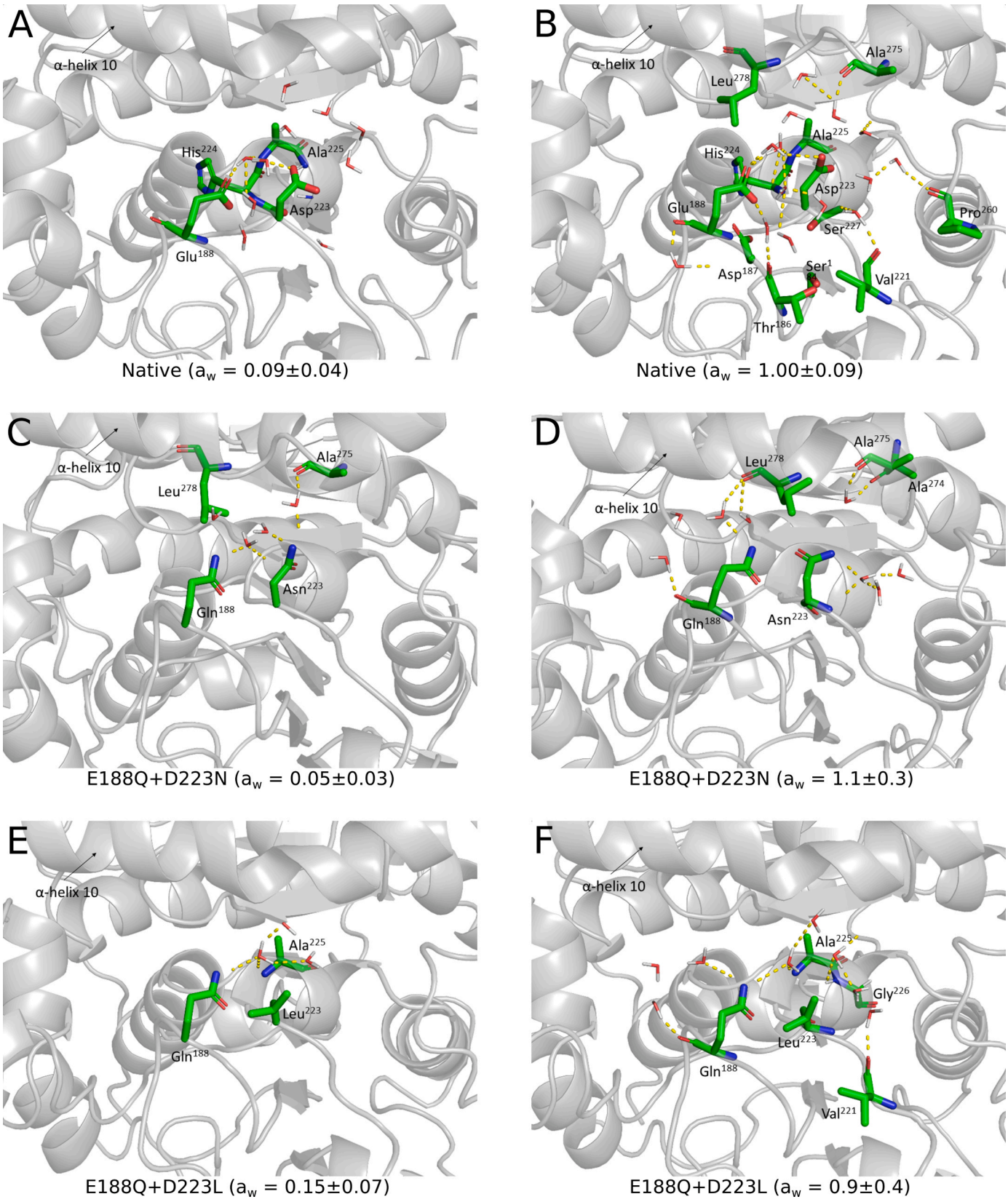

Fig. 2. Water cluster formation around residue 188 and residue 223. The last frame from the simulations of $CALB^{native}$ (A+B), $CALB^{E188Q+D223N}$ (C+D), and $CALB^{E188Q+D223L}$ (E + F) at low (100 H_2O) and high (300 H_2O) water activity is used to visualise the change in the water cluster.

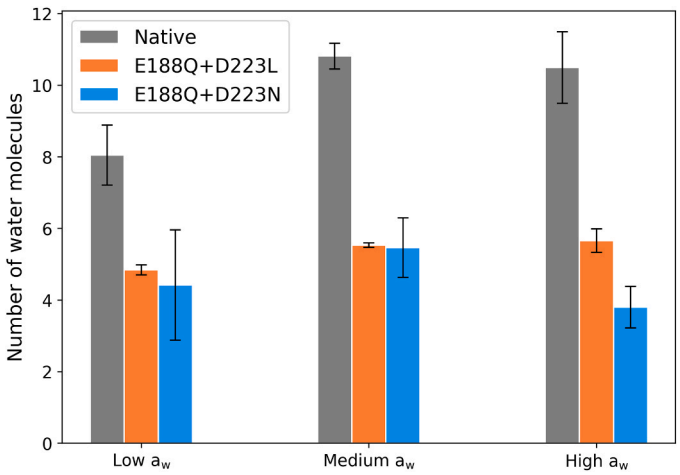

Fig. 3. Number of water molecules in contact with residue 188 and residue 223 at low ($a_w \approx 0.1$, 100 H_2O), medium ($a_w \approx 0.6$, 200 H_2O) and high a_w ($a_w \approx 1.0$, 300 H_2O). Data are shown for $CALB^{native}$ (grey), $CALB^{E188Q+D223L}$ (orange), and $CALB^{E188Q+D223N}$ (blue).

conformation is maintained during catalysis, the esterification reaction can occur. Additional MD simulations were carried out on the lipase-substrate complexes to study the active site arrangements. CALB catalyses the esterification reaction between butyric acid and ethanol by a ping-pong bi-bi mechanism, where a proton transfer between His^{224} and Ser^{105} activates the serine, which can then attack the carboxyl group of butyric acid. [71] The reaction yields a water molecule. The resulting tetrahedral intermediate is afterwards attacked by ethanol, releasing the product (ethyl butyrate) and regenerating the lipase. Since butyric acid is the first substrate to enter the active site, additional MD simulations were performed on $CALB^{native}$, $CALB^{E188Q+D223N}$, and $CALB^{E188Q+D223L}$ where a butyric acid molecule was docked into the active sites. We investigated the distance between Ser^{105}(OG; pdb atom type notation) and His^{224}(NE2) together with the distance between the carboxyl carbon in butyric acid and Ser^{105}(OG). The results are summarised in Table 2 and Fig. 5. Vetrano and co-workers performed an *in-silico* study of CALB in 30% acetonitrile and 30% *tert*-butanol and found that the active site could have different conformations. [67] A distance of 3.0 Å between Ser^{105}(OG) and His^{224}(NE2) corresponded to a direct hydrogen bond between the two residues, while a distance of 4.0 Å corresponded to a water-mediated hydrogen bond, where the required proton transfer between serine and histidine was possible through a Grotthus mechanism. [72] Lastly, they observed that distances above 4.5 Å corresponded to a broken hydrogen bond. From our MD simulations, we propose that the distance between Ser^{105}(OG) and carboxyl carbon in butyric acid should be around 4.0 Å, while Ser^{105} and His^{224} should be either 3.0 Å or 4.0 Å apart for the esterification reaction to occur.

As seen in Table 2 and Fig. 5, $CALB^{native}$ may catalyse the reaction through direct and water-mediated hydrogen bonds. The amount of time $CALB^{native}$ has a competent active site conformation decreases from 41.1% at low a_w to 12.7% at high a_w. This correlates well with the decrease in $CALB^{native}$'s specific activity when a_w increases. [22,23] Interestingly, the amount of time $CALB^{E188Q+D223L}$ has a competent active site arrangement increases from 30.05% at low a_w, to 47.58% at medium a_w, and to 61.02% at high a_w. This suggests that the activity of $CALB^{E188Q+D223L}$ may be positively affected by increasing a_w. The same gradual increase is not seen in $CALB^{E188Q+D223N}$.

3.2. Correlation to experimental enzyme kinetics

From our computational results, we propose that the combination of the four criteria: (*i*) stability, (*ii*) limited water cluster formation, (*iii*)

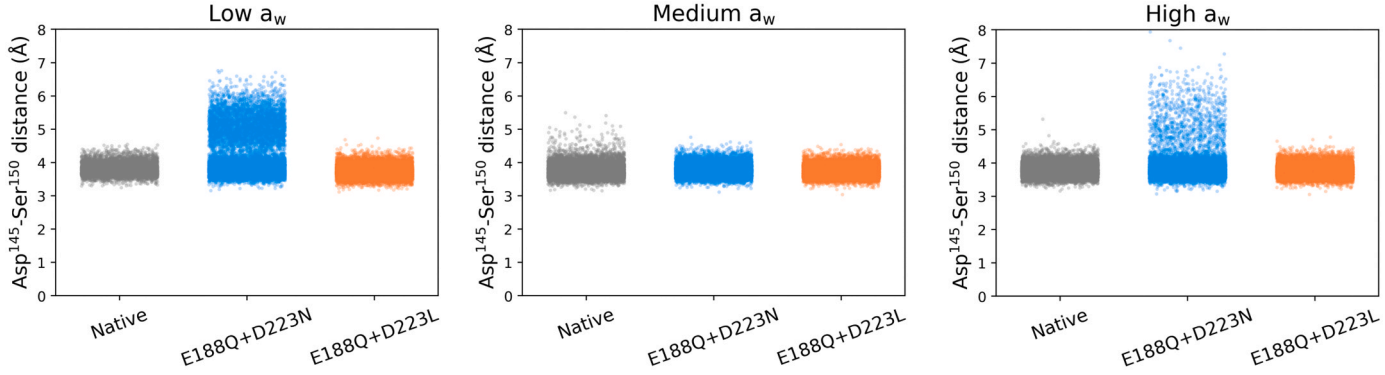

Fig. 4. Distance between Asp^{145}(CG; pdb atom type notation) and Ser^{150}(OG) at low ($a_w \approx 0.1$, 100 H_2O), medium ($a_w \approx 0.6$, 200 H_2O) and high a_w ($a_w \approx 1.0$, 300 H_2O) monitored during the simulations. The distance between Asp^{145} and Ser^{150} represents movement of α-helix 5 going from an open (around 3.75 Å) to a closed (around 7.0 Å) conformation. Each point on the plot corresponds to a conformation during the simulations. The time evolution of the distance in $CALB^{E188Q+D223N}$ is presented in Fig. S5.

Table 2
Percentages of time $CALB^{native}$ and the two mutants have an active site arrangement competent for catalysis.

Lipase	Number of H_2O^a	a_w	Direct H-bond	Water mediated H-bond	Total
$CALB^{native}$	100	0.09 ± 0.04	31.13%	9.97%	41.10%
	200	0.6 ± 0.4	6.12%	15.90%	22.02%
	300	1.00 ± 0.09	4.13%	8.62%	12.74%
$CALB^{E188Q+D223N}$	100	0.05 ± 0.03	2.17%	13.47%	15.64%
	200	0.6 ± 0.1	4.15%	8.20%	12.35%
	300	1.1 ± 0.3	51.95%	3.23%	55.18%
$CALB^{E188Q+D223L}$	100	0.15 ± 0.07	27.87%	2.18%	30.05%
	200	0.6 ± 0.4	37.25%	10.33%	47.58%
	300	0.9 ± 0.4	54.50%	6.52%	61.02%

a 100, 200, and 300 water molecules correspond to low, medium, and high water activities, respectively.

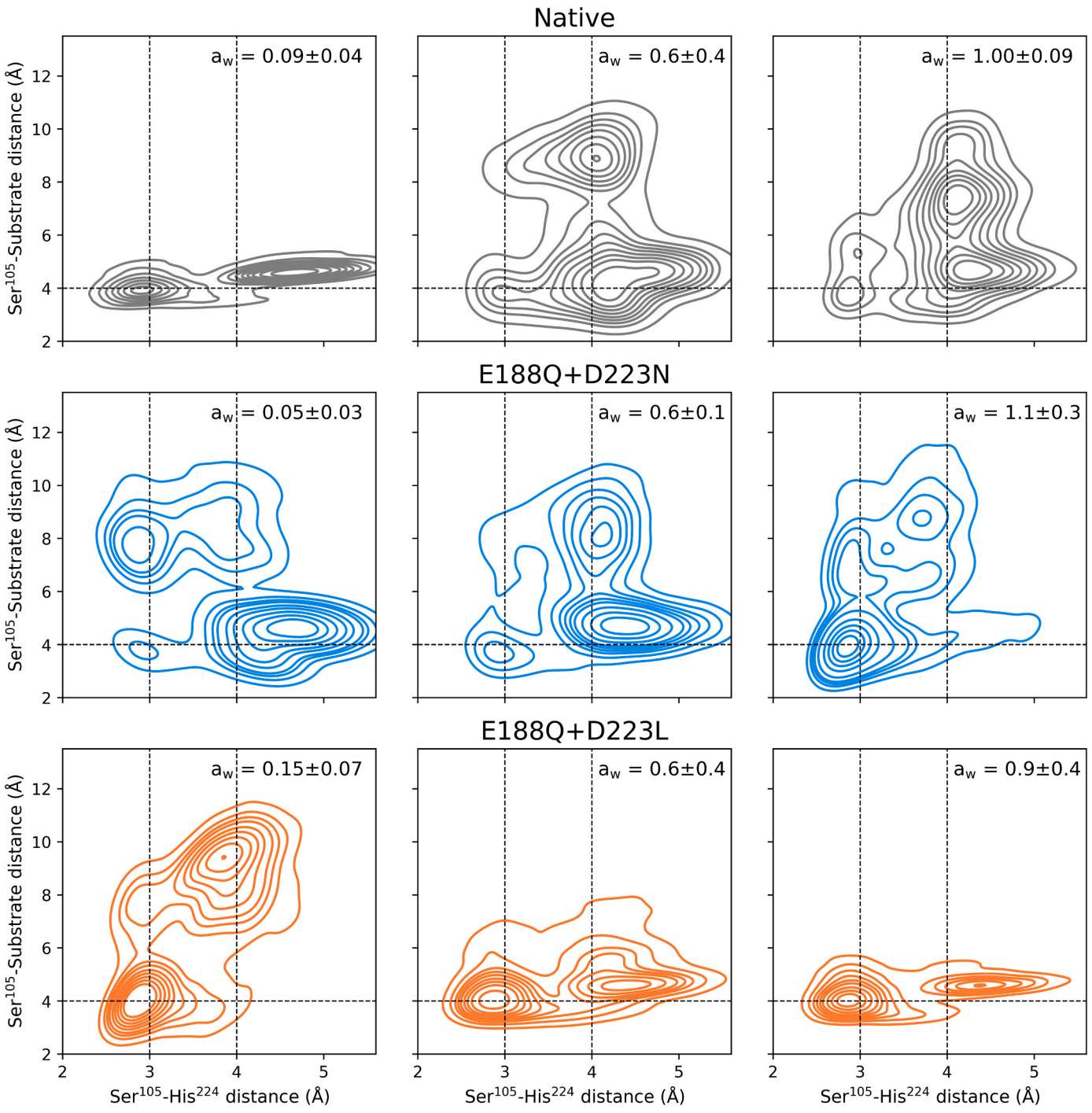

Fig. 5. Conformation of the active site in CALB^{native} (top panels), CALB$^{E188Q+D223N}$ (middle panels), and CALB$^{E188Q+D223L}$ (bottom panels) at different a_w. A distance between Ser^{105}(OG) and His^{224}(NE2) of 3.0 Å corresponds to a direct hydrogen bond, while a distance of 4.0 Å is a water-mediated hydrogen bond. A distance of 4.0 Å between Ser^{105}(OG) and carboxyl carbon in butyric is optimal for catalysis.

open lid conformation, (*iv*) and catalytically competent conformation of the activity site residues and substrate can explain whether CALB-catalysed synthesis can occur in an organic solvent, and whether it is affected by a_w. To test the hypothesis based on the computational findings, the specific activities of CALB^{native} and the mutants, CALB$^{E188Q+D223N}$ and CALB$^{E188Q+D223L}$, were examined in hexane at water activities ranging from 0.12 to 0.97. The esterification reaction between butyric acid and ethanol, producing ethyl butyrate, was used as a model system. The specific activities of the CALB^{native} and the two CALB mutants were determined using the initial reaction rate as described in the Materials and Methods section (subsection 2.2.3). As seen in Fig. 6, the activity of CALB^{native} decreases from 17 to 11 mmol/min/mg as a_w increases. The same trend has previously been shown in MTBE and ACN for soluble as well as immobilised CALB, as summarised in Table S1. [22,23] CALB^{native}'s activity profile fits well with the computationally observed water cluster formation and growth, and supports the hypothesis that the water cluster may potentially block the substrates' path to the active site. [23] In addition, the MD simulations revealed that its active site became less competent for catalysis, as a_w increases (Fig. 5).

In comparison to CALB^{native}, the activity of CALB$^{E188Q+D223N}$ is largely unaffected by a_w, while, interestingly, the activity of CALB$^{E188Q+D223L}$ even seems to rise with increasing a_w. These observations

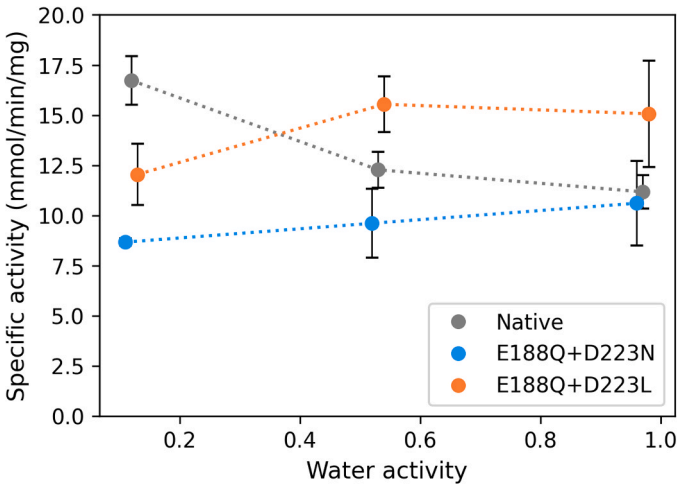

Fig. 6. Specific activities of CALB^{native} and the two mutants, CALB$^{E188Q+D223N}$ and CALB$^{E188Q+D223L}$, in hexane. The specific activities were calculated based on duplicate experiments.

support the hypothesis that Glu^{188} and Asp^{223} facilitate the water cluster formation close to the active site, and that water cluster growth in this area can negatively affect CALB's activity. The enzyme kinetics assay indicates that CALB$^{E188Q+D223N}$ is less active than CALB$^{E188Q+D223L}$. From the MD simulations, it is seen that the lid in CALB$^{E188Q+D223N}$ is more dynamic favouring a closed conformation when compared with CALB$^{E188Q+D223L}$ which adopts a more open conformation (Fig. 4). In addition, studying the active site conformations revealed that CALB$^{E188Q+D223L}$ has a more competent arrangement for catalysis compared to CALB$^{E188Q+D223N}$ (Table 2 and Fig. 5).

4. Conclusion

In this study, we have investigated the effect of water activity on CALB^{native} and two mutated variants, CALB$^{E188Q+D223N}$ and CALB$^{E188Q+D223L}$, in hexane using molecular dynamics simulations. We proposed four criteria for lipase activity in non-aqueous systems: i) the lipase must be stable in the reaction medium; ii) no hindrance for substrate molecule to enter the active site from water clusters on the protein surface; iii) an open lid conformation; and iv) a catalytically competent active site arrangement. The MD simulations revealed that water cluster formation close to the active site is facilitated by Glu^{188} and Asp^{223}, and mutating these residues can reduce the water cluster formation, which may have a positive effect on the lipase activity at high a_w. In addition, results from the MD simulations suggest that lid movements and the geometry of the active site also affect the lipase activity. To support our hypothesis, the specific activities of CALB^{native}, CALB$^{E188Q+D223N}$, and CALB$^{E188Q+D223L}$ in hexane were determined using an enzyme kinetics assay. Whereas CALB^{native}, as seen before, showed a clear decrease in specific activity with increasing water activity, both mutants behaved differently with unaffected or even increasing specific activity (most significant for CALB$^{E188Q+D223L}$). The broader scope of this approach remains to be validated in other systems (other enzymes, reactions, media). However, we suggest that these criteria may be employed to understand specifically lipase reactions in organic solvents, but also further to streamline the process of designing enzymes appropriate for industrial use.

Funding

This research was funded by the Independent Research Fund Denmark (DFF); project number 0136-00111B.

CRediT authorship contribution statement

Helena D. Tjørnelund: Conceptualization, Methodology, Investigation, Writing – original draft, Writing – review & editing, Visualization. **Jesper Vind**: Methodology, Writing – review & editing. **Jesper Brask**: Conceptualization, Methodology, Writing – review & editing, Supervision. **John M. Woodley**: Conceptualization, Methodology, Resources, Writing – review & editing, Supervision. **Günther H.J. Peters:** Conceptualization, Methodology, Resources, Writing – review & editing, Supervision, Project administration, Funding acquisition.

Declaration of Competing Interest

The authors declare that there are no known conflicts of interest. The financial support of the research or personal relationships do not have any significant impact on the outcomes reported in this work.

Appendix A. Supporting information

Supplementary data associated with this article can be found in the online version at doi:10.1016/j.csbj.2023.10.049.

References

[1] Sym EA Über. Die Esterasewirkung III. Biochem Z 1933;258:304–24.
[2] Sym EA Eine. Methode Der Enzymatischen Estersynthesen. Enzymologia 1936;1:156–60.
[3] Halling P, Kvittingen L. Why did biocatalysis in organic media not take off in the 1930s? Trends Biotechnol 1999;17(9):343–4. https://doi.org/10.1016/S0167-7799(99)01331-1.
[4] Klibanov AM. Answering the question: 'why did biocatalysis in organic media not take off in the 1930s? Trends Biotechnol 2000;18(3):85–6. https://doi.org/10.1016/S0167-7799(99)01404-3.
[5] Zaks A, Klibanov AM. Enzymatic catalysis in organic media at 100°C. Science 1984;224(4654):1249–51. https://doi.org/10.1126/science.6729453.
[6] Zaks A, Klibanov AM. Enzyme-catalyzed processes in organic solvents. PNAS 1985;82(10):3192–6. https://doi.org/10.1073/pnas.82.10.3192.
[7] Rios NS, Pinheiro BB, Pinheiro MP, Bezerra RM, dos Santos JCS, Barros Gonçalves LR. Biotechnological potential of lipases from pseudomonas: sources, properties and applications. Process Biochem 2018;75:99–120. https://doi.org/10.1016/j.procbio.2018.09.003.
[8] Hasan F, Shah AA, Hameed A. Industrial applications of microbial lipases. Enzym Micro Technol 2006;39(2):235–51. https://doi.org/10.1016/j.enzmictec.2005.10.016.
[9] Mehta A, Guleria S, Sharma R, Gupta R. The Lipases and Their Applications with Emphasis on Food industry. In Microbial Biotechnology in Food and Health. Elsevier,; 2021. p. 143–64. https://doi.org/10.1016/B978-0-12-819813-1.00006-2.
[10] Sharma R, Chisti Y, Banerjee UC. Production, purification, characterization, and applications of lipases. Biotechnol Adv 2001;19(8):627–62. https://doi.org/10.1016/S0734-9750(01)00086-6.
[11] Gurung N, Ray S, Bose S, Rai V. A broader view: microbial enzymes and their relevance in industries, medicine, and beyond. Biomed Res Int 2013;2013:329121. https://doi.org/10.1155/2013/329121.
[12] Li Q, Yan Y. Production of biodiesel catalyzed by immobilized pseudomonas cepacia lipase from Sapium Sebiferum Oil in Micro-Aqueous Phase. Appl Energy 2010;87(10):3148–54. https://doi.org/10.1016/j.apenergy.2010.02.032.
[13] Sharma S, Kanwar SS. Organic solvent tolerant lipases and applications. Sci World J 2014;2014:625258. https://doi.org/10.1155/2014/625258.
[14] Wong H, Schotz MC. The lipase gene family. J Lipid Res 2002;43(7):993–9. https://doi.org/10.1194/jlr.R200007-JLR200.
[15] Lotti, M., Alberghina, L. Lipases: Molecular Structure and Function. In Industrial Enzymes; Springer Netherlands: Dordrecht; pp 263–281. https://doi.org/10.1007/1–4020-5377–0_16.
[16] Wang X, Liu K, Wang Y, Huang Z, Wang X. Preparation of 2-Arachidonoylglycerol by enzymatic alcoholysis: effects of solvent and water activity on acyl migration. Foods 2022;11(20):3213. https://doi.org/10.3390/foods11203213.
[17] Wehtje E, Adlercreutz P. Lipases have similar water activity profiles in different reactions. Biotechnol Lett 1997;11(6):537–40. https://doi.org/10.1023/A:1018385203375.
[18] Valivety RH, Halling PJ, Peilow AD, Macrae AR. Lipases from different sources vary widely in dependence of catalytic activity on water activity. Biochim Et Biophys Acta (BBA) Protein Struct Mol Enzymol 1992;1122(2):143–6. https://doi.org/10.1016/0167-4838(92)90316-6.
[19] Valivety RH, Halling PJ, Macrae AR. Effect of water activity on rate of lipase catalysed esterification. Prog Biotechnol 1992;Vol. 8:549–55. https://doi.org/10.1016/B978-0-444-89046-7.50080-1.

[20] Schmitke JL, Wescott CR, Klibanov AM. The mechanistic dissection of the plunge in enzymatic activity upon transition from water to anhydrous solvents. J Am Chem Soc 1996;118(14):3360–5. https://doi.org/10.1021/ja9539958.

[21] Bracco P, van Midden N, Arango E, Torrelo G, Ferrario V, Gardossi L, et al. Bacillus subtilis lipase A—Lipase or Esterase? Catalysts 2020;10(3):308. https://doi.org/10.3390/catal10030308.

[22] Tjørnelund HD, Brask J, Woodley JM, Peters GHJ. Optimised protocol for drying aqueous enzyme solutions in organic solvents – comparison of free and immobilised *Candida Antarctica* Lipase B. ChemCatChem 2023;15(1). https://doi.org/10.1002/cctc.202201207.

[23] Dutta Banik S, Nordblad M, Woodley JM, Peters GHJ. Effect of water clustering on the activity of Candida Antarctica Lipase B in Organic Medium. Catalysts 2017;7(8):227. https://doi.org/10.3390/catal7080227.

[24] Ingenbosch KN, Vieyto-Nuñez JC, Ruiz-Blanco YB, Mayer C, Hoffmann-Jacobsen K, Sanchez-Garcia E. Effect of organic solvents on the structure and activity of a minimal lipase. JOC 2022;87(3):1669–78. https://doi.org/10.1021/acs.joc.1c01136.

[25] Dutta Banik S, Nordblad M, Woodley JM, Peters GHJ. A correlation between the activity of Candida Antarctica Lipase B and differences in binding free energies of organic solvent and substrate. ACS Catal 2016;6(10):6350–61. https://doi.org/10.1021/acscatal.6b02073.

[26] Olofsson L, Nicholls IA, Wikman S. TBADH Activity in water-miscible organic solvents: correlations between enzyme performance, enantioselectivity and protein structure through spectroscopic studies. Org Biomol Chem 2005;3(5):750. https://doi.org/10.1039/b418040b.

[27] Watanabe K, Yoshida T, Ueji S. The role of conformational flexibility of enzymes in the discrimination between amino acid and ester substrates for the subtilisin-catalyzed reaction in organic solvents. Bioorg Chem 2004;32(6):504–15. https://doi.org/10.1016/j.bioorg.2004.05.001.

[28] Trodler P, Pleiss J. Modeling structure and flexibility of Candida Antarctica Lipase B in organic solvents. BMC Struct Biol 2008;8. https://doi.org/10.1186/1472-6807-8-9.

[29] Idris A, Bukhari A. Immobilized Candida Antarctica Lipase B: hydration, stripping off and application in ring opening polyester synthesis. Biotechnol Adv 2012;30(3):550–63. https://doi.org/10.1016/j.biotechadv.2011.10.002.

[30] Wedberg R, Abildskov J, Peters GH. Protein dynamics in organic media at varying water activity studied by molecular dynamics simulation. J Phys Chem B 2012;116(8):2575–85. https://doi.org/10.1021/jp211054u.

[31] Case, D.A., Ben-Shalom, I.Y., Brozell, S.R., Cerutti, D.S., Cheatham, T.E. (III), Cruzeiro, V.W.D., Darden, T.A., Duke, R.E., Ghoreishi, D., Giambasu, G., Giese, T., Gilson, M.K., Gohlke, H., Goetz, A.W., Greene, D., Harris, R., Homeyer, N., Huang, Y., Izadi, S., Kovalenko, A., Krasny, R., Kurtzman, T., Lee, T.S., LeGrand, S., Li, P., Lin, C., Liu, J., Luchko, T., Luo, R., Man, V., Mermelstein, D.J., Merz, K.M., Miao, Y., Monard, G., Nguyen, C., Nguyen, H., Onufriev, A., Pan, F., Qi, R., Roe, D.R., Roitberg, A., Sagui, C., Schott-Verdugo, S., Shen, J., Simmerling, C.L., Smith, J., Swails, J., Walker, R.C., Wang, J., Wei, H., Wilson, L., Wolf, R.M., Wu, X., Xiao, L., Xiong, Y., York, D.M., Kollman, P.A. AMBER 2019; University of California: San Francisco, 2019.

[32] PubChem Compound Summary for CID 8058, Hexane. National Center for Biotechnology Information. https://pubchem.ncbi.nlm.nih.gov/compound/Hexane (accessed 2022-08–21).

[33] Wang J, Wolf RM, Caldwell JW, Kollman PA, Case DA. Development and testing of a general amber force field. J Comput Chem 2004;25(9):1157–74. https://doi.org/10.1002/jcc.20035.

[34] Martínez L, Andrade R, Birgin EG, Martínez JM. PACKMOL: a package for building initial configurations for molecular dynamics simulations. J Comput Chem 2009;30(13):2157–64. https://doi.org/10.1002/jcc.21224.

[35] Stauch B, Fisher SJ, Cianci M. Open and Closed States of Candida Antarctica Lipase B: protonation and the mechanism of interfacial activation. J Lipid Res 2015;56(12):2348–58. https://doi.org/10.1194/jlr.M063388.

[36] Uppenberg J, Hansen MT, Patkar S, Jones TA. The sequence, crystal structure determination and refinement of two crystal forms of lipase B from Candida Antarctica. Structure 1994;2(4):293–308. https://doi.org/10.3168/jds.S0022-0302(88)79885-9.

[37] Berman HM, Westbrook J, Feng Z, Gilliland G, Bhat TN, Weissig H, et al. The protein data bank. Nucleic Acids Res 2000;28(1):235–42.

[38] Gordon JC, Myers JB, Folta T, Shoja V, Heath LS, Onufriev A. H++: A server for estimating pkas and adding missing hydrogens to macromolecules. Nucleic Acids Res 2005;33:W368–71.

[39] Anandakrishnan R, Aguilar B, Onufriev AV. H++ 3.0: Automating PK prediction and the preparation of biomolecular structures for atomistic molecular modeling and simulations. Nucleic Acids Res 2012;40(W1):537–41. https://doi.org/10.1093/nar/gks375.

[40] Myers J, Grothaus G, Narayanan S, Onufriev A. A simple clustering algorithm can be accurate enough for use in calculations of PKs in macromolecules. Proteins 2006;63(4):928–38. https://doi.org/10.1002/prot.20922.

[41] Wohlfarth Ch. In: Lechner MD, editor. Dielectric Constant of Hexane. Berlin Heidelberg: Springer-Verlag; 2008. p. 360–2. https://doi.org/10.1007/978-3-540-75506-7_204.

[42] Jorgensen WL, Chandrasekhar J, Madura JD, Impey RW, Klein ML. Comparison of simple potential functions for simulating liquid water. J Chem Phys 1983;79(2):926–35. https://doi.org/10.1063/1.445869.

[43] Maier JA, Martinez C, Kasavajhala K, Wickstrom L, Hauser KE, Simmerling C. Ff14SB: improving the accuracy of protein side chain and backbone parameters from Ff99SB. J Chem Theory Comput 2015;11(8):3696–713. https://doi.org/10.1021/acs.jctc.5b00255.

[44] Li C, Tan T, Zhang H, Feng W. Analysis of the conformational stability and activity of Candida Antarctica Lipase B in Organic Solvents. Insight Mol Dyn Quantum Mech/Simul JBC 2010;285(37):28434–41. https://doi.org/10.1074/jbc.M110.136200.

[45] Braun E, Gilmer J, Mayes HB, Mobley DL, Monroe JI, Prasad S, et al. Best practices for foundations in molecular simulations [Article v1.0]. Living J Comput Mol Sci 2019;1(1). https://doi.org/10.33011/livecoms.1.1.5957.

[46] Pastor RW, Brooks BR, Szabo A. An analysis of the accuracy of langevin and molecular dynamics algorithms. Mol Phys 1988;65(6):1409–19. https://doi.org/10.1080/00268978800101881.

[47] Åqvist J, Wennerström P, Nervall M, Bjelic S, Brandsdal BO. Molecular dynamics simulations of water and biomolecules with a monte carlo constant pressure algorithm. Chem Phys Lett 2004;384(4–6):288–94. https://doi.org/10.1016/j.cplett.2003.12.039.

[48] Darden T, York D, Pedersen L. Particle Mesh Ewald: An N ·log(N) Method for Ewald Sums in Large Systems. J Chem Phys 1993;98(12):10089–92. https://doi.org/10.1063/1.464397.

[49] Ryckaert J-P, Ciccotti G, Berendsen HJC. Numerical integration of the cartesian equations of motion of a system with constraints: molecular dynamics of n-Alkanes. J Comput Phys 1977;23(3):327–41. https://doi.org/10.1016/0021-9991(77)90098-5.

[50] Lu C, Wu C, Ghoreishi D, Chen W, Wang L, Damm W, et al. OPLS4: Improving force field accuracy on challenging regimes of chemical space. J Chem Theory Comput 2021;17(7):4291–300. https://doi.org/10.1021/acs.jctc.1c00302.

[51] Friesner RA, Banks JL, Murphy RB, Halgren TA, Klicic JJ, Mainz DT, et al. Glide: A new approach for rapid, accurate docking and scoring. 1. Method and assessment of docking accuracy. J Med Chem 2004;47(7):1739–49. https://doi.org/10.1021/jm0306430.

[52] Friesner RA, Murphy RB, Repasky MP, Frye LL, Greenwood JR, Halgren TA, et al. Extra Precision Glide: docking and scoring incorporating a model of hydrophobic enclosure for protein−ligand complexes. J Med Chem 2006;49(21):6177–96. https://doi.org/10.1021/jm051256o.

[53] Roe DR, Cheatham TE. PTRAJ and CPPTRAJ: software for processing and analysis of molecular dynamics trajectory data. J Chem Theory Comput 2013;9(7):3084–95. https://doi.org/10.1021/ct400341p.

[54] Humphrey W, Dalke A, Schulten K. VMD - Visual Molecular Dynamics. J Molec Graph 1996;14:33–8.

[55] Frenkel, D., Smit, B. Understanding Molecular Simulation, Second edition.; Elsevier, 2002. https://doi.org/10.1016/B978-0-12–267351-1.X5000–7.

[56] Steinbrecher T, Mobley DL, Case DA. Nonlinear scaling schemes for lennard-jones interactions in free energy calculations. J Chem Phys 2007;127(21). https://doi.org/10.1063/1.2799191.

[57] Wilding, W.V., Knotts, T.A., Giles, N.F., Rowley, R.L. DIPPR Data Compilation of Pure Chemical Properties. Design Institute for Physical Properties, AIChE: New York 2020.

[58] Skjøt M, de Maria L, Chatterjee R, Svendsen A, Patkar SA, Østergaard PR, et al. Understanding the plasticity of the α/β Hydrolase Fold: lid swapping on the Candida Antarctica Lipase B results in chimeras with interesting biocatalytic properties. ChemBioChem 2009;10(3):520–7. https://doi.org/10.1002/cbic.200800668.

[59] Gasteiger E, Hoogland C, Gattiker A, Duvaud S, Wilkins MR, Appel RD, et al. Protein Identification and Analysis Tools on the ExPASy Server. In: Walker JM, editor. In *The Proteomics Protocols Handbook*. Humana Press: Totowa, New Jersey; 2005. p. 571–607.

[60] Brooks, H.B., Geeganage, S., Kahl, S.D., Montrose, C., Sittampalam, S., Smith, M. C., et al. Basics of Enzymatic Assays for HTS. In Assay Guidance Manual; Markossian, S., Ed.; 2012; pp 93–104.

[61] Kumar A, Dhar K, Kanwar SS, Arora PK. Lipase catalysis in organic solvents: advantages and applications. Biol Proced Online 2016;18(1):2. https://doi.org/10.1186/s12575-016-0033-2.

[62] Salihu A, Alam MZ. Solvent tolerant lipases: a review. Process Biochem 2015;50(1):86–96. https://doi.org/10.1016/J.PROCBIO.2014.10.019.

[63] Skjold-Jørgensen J, Vind J, Moroz OV, Blagova E, Bhatia VK, Svendsen A, et al. Controlled lid-opening in thermomyces lanuginosus lipase– an engineered switch for studying lipase function. Biochim Et Biophys Acta (BBA) - Proteins Proteom 2017;1865(1):20–7. https://doi.org/10.1016/j.bbapap.2016.09.016.

[64] Rehm S, Trodler P, Pleiss J. Solvent-induced lid opening in lipases: a molecular dynamics study. Protein Sci 2010;19(11):2122–30. https://doi.org/10.1002/pro.493.

[65] Tjørnelund HD, Madsen JJ, Peters GHJ. Water-intake and water-molecule paths to the active site of secretory phospholipase A 2 studied using MD simulations and the tracking tool AQUA-DUCT. J Phys Chem B 2020;124(10):1881–91. https://doi.org/10.1021/acs.jpcb.9b10837.

[66] Linderoth L, Fristrup P, Hansen M, Melander F, Madsen R, Andresen TL, et al. Mechanistic study of the SPLA2-mediated hydrolysis of a thio-ester pro anticancer ether lipid. J Am Chem Soc 2009;131(34):12193–200. https://doi.org/10.1021/ja901412j.

[67] Vetrano A, Daidone I, Spreti N, Capone M. A Combined experimental and computational approach for the rationalization of the catalytic activity of lipase B from Candida Antarctica in water–organic solvent mixtures. JCTB 2023. https://doi.org/10.1002/jctb.7467.

[68] Yennawar, N.H.; Yennawar, H.P.; Farber, G.K. X-Ray Crystal Structure of-Chymotrypsin in Hexane; 1994; Vol. 33. https://pubs.acs.org/sharingguidelines.

[69] Gao, X.-G., Maldonado, E., Pérez-Montfort, R., Garza-Ramos, G., De Gomezgomez-Puyou, M.T., Gomezgomez-Puyou, A., et al. Crystal Structure of Triosephosphate Isomerase from Trypanosoma Cruzi in Hexane; 1999; Vol. 96. www.pnas.org.

[70] Nazarian Z, Arab SS. Solvent-dependent activity of Candida Antarctica lipase B and its correlation with a regioselective mono aza-michael addition - experimental and molecular dynamics simulation studies. Heliyon 2022;8(8). https://doi.org/10.1016/j.heliyon.2022.e10336.

[71] Zaidi A, Gainer JL, Carta G, Mrani A, Kadiri T, Belarbi Y, et al. Esterification of fatty acids using nylon-immobilized lipase in n-Hexane: kinetic parameters and chain-length effects. J Biotechnol 2002;93(3):209–16. https://doi.org/10.1016/S0168-1656(01)00401-1.

[72] Agmon N. The grotthuss mechanism. Chem Phys Lett 1995;244(5–6):456–62. https://doi.org/10.1016/0009-2614(95)00905-J.